

Walk through Paintings: Egocentric World Models from Internet Priors

Anurag Bagchi¹ Zhipeng Bao¹ Homanga Bharadhwaj¹
 Yu-Xiong Wang² Pavel Tokmakov^{3*} Martial Hebert^{1*}

¹Carnegie Mellon University ²University of Illinois Urbana-Champaign ³Toyota Research Institute

egowm.github.io

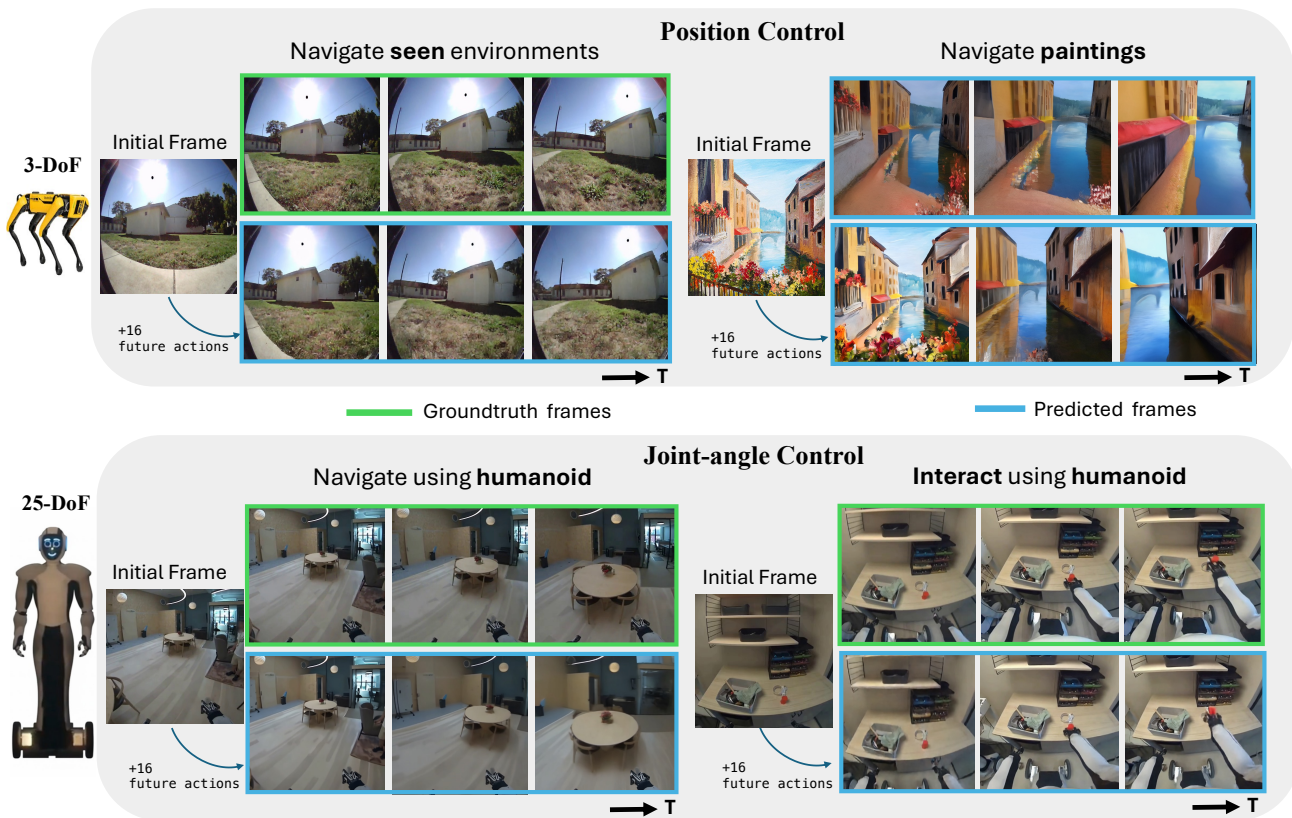


Figure 1. Our framework generates future frame predictions (shown in blue) that accurately follow the provided robot actions (ground-truth frames shown in green). Notably, it effortlessly generalizes to vastly different embodiments, tasks and domains, including non-realistic ones, such as navigating within paintings (top right). This generalization is enabled by our simple, universal architecture.

Abstract

What if a video generation model could not only imagine a plausible future, but the correct one — accurately reflecting how the world changes with each action? We answer this by presenting Egocentric World Model (EgoWM), a simple, architecture-agnostic method that transforms any pre-trained video diffusion model into an action-conditioned

world model, enabling controllable prediction of the future. Rather than training from scratch, we re-purpose the rich world priors of Internet-scale video models, injecting motor commands through lightweight conditioning layers. This allows our model to follow actions faithfully, while preserving generalization and realism. Our approach scales naturally across embodiments and action spaces — from 3-DoF mobile robots to 25-DoF humanoids, where predicting egocentric joint-angle-driven dynamics is substantially more challenging. The model produces coherent rollouts

*Equal advising.

for both navigation and manipulation, requiring only modest fine-tuning. To evaluate physical correctness independent of appearance, we introduce the *Structural Consistency Score (SCS)*, which measures whether stable scene elements evolve consistently with the provided actions. Our method improves SCS by up to 80% over prior state-of-the-art (Navigation World Models) while exhibiting up to 6× lower latency and generalizing robustly to unseen environments — including navigation inside paintings.

1. Introduction

Modeling how the future visual state of the world evolves in response to an agent’s actions – often referred to as *world modeling* [15] – is a fundamental capability for organisms with vision. It enables planning in navigation and manipulation tasks and even creative problem-solving [28, 33]. Animals acquire this ability through a lifetime of interaction and observation of others, allowing us to anticipate outcomes even in novel or physically impossible scenarios.

For artificial agents, however, action-conditioned videos in diverse real-world settings are limited and expensive to acquire – an agent must interact with the world to get this data. As a result, many existing works train world models on narrow, simulator-defined datasets [3, 41] or with bespoke designs [7, 37, 45, 53], which constrains their scalability. This leads to a crucial question: can we re-purpose off-the-shelf video models trained on large-scale *passive* data, and convert them into world models using only a small amount of paired *action–observation* data?

Several prior works have explored learning action-conditioned video prediction models [7, 14, 17, 41, 54]. For example, the recent Navigation World Models (NWM) approach trains a 1-billion-parameter diffusion model on egocentric videos of robots and humans to model navigation behavior. While NWM demonstrates strong cross-environment generalization, collecting large datasets for every new embodiment or domain is impractical. More generally, prior world models in robotics or games remain domain-specific, learned for a single robot or a single environment.

In contrast, large generative video models trained on diverse datasets have shown the ability to visually emulate real-world interactions when given suitable prompts [2, 49]. Our insight is to harness these pre-trained models as a starting point. By fine-tuning them with lightweight conditioning on action inputs, we can enable strong out-of-domain generalization: for instance, our model trained on real videos can simulate plausible navigation in entirely unseen environments, even those that do not exist in reality, thanks to the rich prior learned from internet-scale data.

Specifically, we build on the observation that modern video diffusion architectures use a denoising timestep embedding to control the generation process. We introduce an

action embedding module that piggybacks on this timestep conditioning. In practice, the action at each (latent) frame is encoded and added to the model’s time-conditioning pathway via learned scale-and-shift transformations.

This design is architecture-agnostic: it does not alter the original model’s layers and works across different backbone architectures. We demonstrate this with both a UNet-based [36] diffusion model and a DiT-based (Diffusion Transformer) [32] model. Importantly, our conditioning operates directly in the *joint-angle space* of the robot or humanoid, enabling seamless scaling to complex embodiments with up to 25-*DoF action spaces*. As shown in Figure 1, this makes our method applicable to high-dimensional humanoid navigation and manipulation — a capability not demonstrated by any prior open-source world model. Predicting how a humanoid’s body moves and how the entire visual scene evolves accordingly is significantly harder than predicting SE(3) camera motion. Furthermore, compared to NWM, our model achieves higher spatial resolution and lower latency, making it more practical for real-time, closed-loop deployment.

To quantitatively evaluate our approach, we also propose a new metric: **Structural Consistency Score (SCS)**. Prior metrics such as LPIPS [51] or FVD [40] focus on perceptual similarity or realism [26, 48], which can conflate visual fidelity with physical correctness. A model could produce sharp, realistic frames that nevertheless depict physically inconsistent outcomes. SCS instead measures whether the *structure* of the generated environment evolves correctly in response to the agent’s actions, independent of texture.

Concretely, we automatically identify stable scene structures (*e.g.*, walls, furniture, landmarks) in the first frame and track them across both real and generated videos using a segmentation tracker. Comparing the resulting trajectories allows us to assess whether the model’s predicted world evolves coherently with the true environment. A higher SCS indicates stronger structural and physical consistency with the provided action sequence.

In summary, our contributions are as follows:

- We propose a simple yet powerful recipe to convert pre-trained video diffusion models into **action-conditioned world models**.
- We demonstrate that our method works across architectures and extends seamlessly to **egocentric 25-DoF** humanoids, enabling high-resolution video prediction for navigation and manipulation.
- We introduce the **Structural Consistency Score (SCS)**, a metric for evaluating the structural and physical plausibility of generated videos independent of appearance.

By learning from large-scale passive datasets and a small amount of action-labeled data, our framework offers a path toward scalable, general-purpose visual dynamics models.

2. Related Work

World models and video prediction have long been studied in reinforcement learning and robotics. For example, the classic World of Ha and Schmidhuber [15] trained a variational RNN to simulate simple games, allowing an agent to plan within its own latent dream. Follow-up works demonstrated video prediction for control in robotics – *e.g.*, visual foresight model [11], which learned to predict future camera frames given robot actions and used model-predictive control to push objects to the target location, or SV2P [4], which introduced stochastic latent variables for multi-modal future predictions. These pioneering approaches, however, were limited to relatively constrained environments (toy simulations or single-task robot setups).

In the gaming domain, several works have proposed to visually emulate an entire game engine from screen pixels and keyboard actions [22, 29, 46]. More recently, there is a trend of utilizing high-capacity generative models for world modeling. The DIAMOND agent [3] uses a diffusion-based world model to better preserve visual detail in Atari games. GameNGen [41] takes a similar diffusion-based approach to simulate an entire 3D game in real time. These results underscore the potential of diffusion models to capture complex dynamics, but so far each has been confined to its specific domain, trained from scratch on domain-specific data.

In another line of work, world models have been trained for table-top manipulation scenarios [14, 31, 53, 54], but are focusing on narrow domains with a static camera and custom model design. Very recently, the Navigation World Models (NWM) [7] broadened the scope by training a single diffusion model across a variety of navigation tasks and embodiments. NWM’s large-scale training on diverse data achieved cross-embodiment generalization in navigation. However, NWM still relies on an expensive, in-domain paired action-observation and a custom model (CDiT), limiting its generalization. In this work, we push further on generality: rather than collecting more data or designing a new model, we adapt existing pre-trained models to a wide variety of tasks, from navigation to humanoid manipulation.

GrndCtrl [17] and Ctrl-World [14], are two concurrent works that leverage video generation pretraining for navigation and multi-view table-top manipulation respectively. While the former simply re-uses an existing action-conditioning implementation of Cosmos [2], the later relies on custom, model-specific conditioning design. In contrast, our simple framework is independent of the base video diffusion architecture and supports more complex action spaces, like the whole body joint angles of a humanoid, for both navigation and manipulation from an ego-centric view.

Video diffusion models have emerged as a powerful paradigm for video generation. Ho et al. [18] demonstrated that a straightforward extension of image diffusion models

can produce high-quality short videos. This was followed by text-to-video models leveraging massive paired visual-language samples [8, 10, 44]. These models are trained on observation-only video data (*e.g.*, crawled web videos) and are not inherently action-conditioned, but they learn strong priors about physics and appearances. There have also been advances in architectural design: Diffusion Transformers (DiT) [32] replaced the U-Net [36] backbone, achieving excellent video generation performance [2, 43, 50].

More recently, diffusion-based generative models have been adapted beyond pure synthesis to support downstream vision and control tasks — leveraging their rich priors to enable generalization to unseen domains. For example, in the image domain, several works [21, 25, 30, 52] have shown that a pretrained image diffusion backbone can be used to bring several classic vision tasks into the open world. Video diffusion representations have been successfully adapted for video segmentation [5, 55], dynamic views synthesis [6, 42], as well as for robot policy learning [19, 24], demonstrating never-before-seen levels of generalization for these tasks. In contrast, in world model learning, most of the approaches – while adopting the video diffusion objective – utilize custom model design, limiting the benefits of pre-trained representations.

Evaluation metrics used in video generation were originally designed for image fidelity or distributional similarity. Frame-level measures such as SSIM [47] and PSNR [27] evaluate brightness, contrast, and structure per frame, while LPIPS [51] compares deep features for improved perceptual alignment but lacks temporal awareness. Sequence-level metrics like Fréchet Video Distance (FVD) [40], which measures feature distribution differences using a 3D ConvNet [9], were later introduced to capture temporal quality. World modeling approaches typically adopt these metrics to evaluate predicted futures, yet high scores often fail to reflect action alignment. We address this gap with the Structural Consistency Score (SCS), which explicitly disentangles action-following accuracy from visual fidelity.

3. Method

3.1. Preliminaries

Modern video diffusion models [8, 10] synthesize future frames conditioned on an observed frame x_0 (and optionally texts) by iteratively denoising a Gaussian latent. Let f_{vdm} denote a pre-trained image-to-video model parameterized for T_s diffusion steps. Sampling is performed by drawing $\epsilon \sim \mathcal{N}(0, I)$ and applying the reverse denoising process:

$$\hat{X} = f_{\text{vdm}}(c_t, \epsilon, T_s), \quad (1)$$

where c_t encodes the frame-level conditioning signal.

To reduce computation, these models operate in a low-dimensional latent space. A video $X \in \mathbb{R}^{T \times H \times W \times 3}$ is

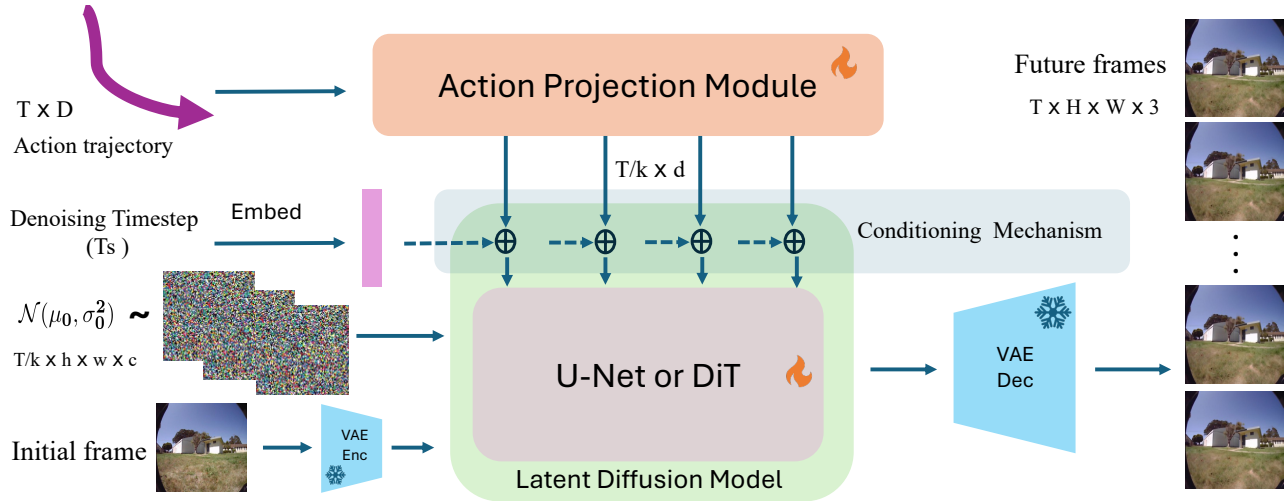


Figure 2. Our method embeds action sequences or arbitrary dimensionality into a universal feature space and injects these embeddings into a pre-trained video diffusion model by reusing its timestep-conditioning pathway (shown in the top center). This enables turning any passive video generation model into a world model without destroying the pre-trained representation.

mapped by a spatio-temporal VAE [23, 35] into a latent tensor $z = \mathcal{E}(X) \in \mathbb{R}^{\frac{T}{k} \times h \times w \times c}$, where k denotes the temporal downsampling factor. Generation proceeds by decoding the predicted latent trajectory:

$$\hat{X} = \mathcal{D}(f_{\text{vdm}}(c_t, \epsilon, T_s)). \quad (2)$$

During training, a noisy latent z_{t_s} is produced by the forward diffusion process, and the model learns to predict the injected noise:

$$\min_{\theta} \mathbb{E}_{z, t_s, \epsilon} \left[\|\epsilon - \epsilon_{\theta}(z_{t_s}, e_c, t_s)\|_2^2 \right]. \quad (3)$$

Here e_c denotes the conditioning embedding and $\epsilon_{\theta}(\cdot)$ is implemented by a U-Net [36] or a DiT-based [32] denoiser. Although architectures vary widely, all models share a common mechanism: latent features are modulated by the denoising timestep t_s , which forms the basis of our action-conditioning strategy.

3.2. Action Conditioning

Our objective is to convert passive, frame-conditioned video diffusion models into action-conditioned world models. Formally, given an action sequence $\mathbf{A} \in \mathbb{R}^{D \times T}$, where D denotes the action-space dimensionality and T the prediction horizon, and an initial observation x_0 , the model is fine-tuned to generate a sequence of future frames:

$$\hat{X}_{1:T} = f_{\text{vdm}}(x_0, \mathbf{A}, \epsilon, T_s). \quad (4)$$

To enable this, we design a general framework, shown in Figure 2, that injects temporally aligned control information into the diffusion process without modifying the base model architecture. This universal design is architecture-agnostic, allowing a single conditioning strategy to generalize across

multiple diffusion models and embodiments. Next, we describe the key components of our approach in more detail.

Action projection. To condition a video diffusion model on a control trajectory \mathbf{A} , we first embed each D -dimensional action vector into a latent representation $\mathbf{Z}_A \in \mathbb{R}^{d \times T}$, where d is the embedding dimension. In its general form, the module, shown in the upper part of Figure 2, consists of a sequence of lightweight multi-layer perceptrons (MLPs) that map each action vector to the embedding space. For video diffusion models that use temporal latent compression (*i.e.*, VAEs with factor $k > 1$), action embeddings are further downsampled by 1D convolutions, producing $\mathbf{Z} \in \mathbb{R}^{d \times T/k}$ to ensure alignment with the latent video frame rate.

Different embodiments use different parameterizations: for *3-DoF Navigation*, we adopt the standard control representation $(\Delta x, \Delta y, \Delta \phi)$; for *25-DoF Humanoid Control*, the standard representation is adopted from [1], but otherwise our design is left unchanged. Because the projection module operates independently of the base architecture and only interfaces through the shared latent space, it can adapt to different temporal resolutions, action dimensionalities, and embodiment types without architectural changes.

Injecting actions via timestep modulation. Given the action embeddings \mathbf{Z}_A , our goal is to modulate the latent representation of the video diffusion model so that the generated frames evolve consistently with the underlying action sequence. We observe that across all video diffusion architectures, the denoising timestep embedding t_s is used to modulate the network’s activations.

Rather than introducing model-specific conditioning layers, as done in some prior works [14, 54], we take advantage of this universal pathway instead: at every location where the model applies a timestep-dependent modulation,

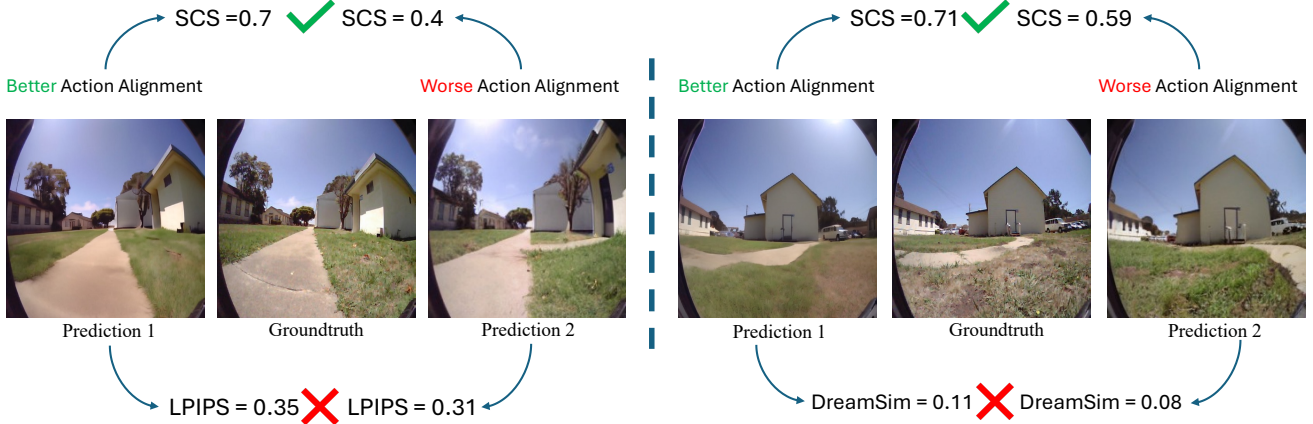


Figure 3. Each column shows two generated rollouts compared to the corresponding ground-truth frame, with their LPIPS, DreamSim, and SCS scores. Perceptual metrics incorrectly favor the visually sharper but physically inconsistent sample, while SCS correctly identifies the sequence that follows the true action trajectory, accurately capturing structural consistency.

we add the corresponding action embedding (shown in Figure 2, middle). Formally, for each modulation block i , we redefine:

$$P_i^{\text{scale}}, P_i^{\text{shift}}, P_i^{\text{gate}} = F_i(Z_{t_s} + Z_a), \quad (5)$$

where Z_{t_s} is the timestep embedding of t_s , and $F_i(\cdot)$ is the block-specific projection used by the base model. For humanoid control, where many body parts are not visible in the camera view, we additionally include the embedding of the initial agent state (obtained by the same projection mechanism) Z_s :

$$P_i^{\text{scale}}, P_i^{\text{shift}}, P_i^{\text{gate}} = F_i(Z_{t_s} + Z_a + Z_s). \quad (6)$$

This simple additive formulation makes the modulation parameters frame-specific and action-aligned, while preserving architectural compatibility with both U-Net-based and DiT-based video diffusion models. Despite its simplicity, this strategy yields fine-grained motion control in both low-DoF and high-DoF settings, demonstrating that an action signal can be injected effectively through the existing timestep-conditioning pathway.

4. Structural Consistency Score

Existing action-conditioned video generation models are typically evaluated using perceptual similarity metrics such as LPIPS [51] or DreamSim [13], computed between the generated and ground-truth frames [7]. While effective for measuring visual fidelity, these metrics were designed to capture semantic similarity between object-centric images, not structural alignment in complex scenes. As shown in Figure 3, two model predictions can achieve similar perceptual similarity scores despite very different action-following behavior. Moreover, applying per-frame similarity metrics to long-horizon navigation ignores the inherent stochasticity of future outcomes: early in a trajectory, a model can

meaningfully reconstruct the ground truth, but as the agent moves farther, multiple plausible futures emerge.

To address these limitations and accurately evaluate action following, we introduce a new metric called **SCS** (Structural Consistency Score). To compute SCS, we first trim each evaluation sequence to exclude frames containing only novel regions unseen in the initial observation, since structural correspondence is ill-defined there. We detect this transition automatically using the dense point tracking method of Harley et al. [16], to identify when all points visible in the first frame have left the field of view.

For the remaining frames, we manually mark key scene structures — static objects whose apparent motion stems solely from the agent’s ego-motion (e.g., buildings, trees, furniture). Restricting evaluation to passive objects reduces ambiguity and allows us to leverage recent foundational models for video object segmentation, such as SAM2 [34], which is robust to the artifacts in generated videos. Each selected object is annotated via sparse point clicks and tracked through both ground-truth and predicted sequences.

The final Structural Consistency Score is obtained by averaging mask IoU [12] across all T frames and N tracked objects:

$$\text{SCS} = \frac{1}{NT} \sum_{j=1}^N \sum_{t=1}^T \frac{|\mathcal{M}_{\text{pred}}^{(t,j)} \cap \mathcal{M}_{\text{gt}}^{(t,j)}|}{|\mathcal{M}_{\text{pred}}^{(t,j)} \cup \mathcal{M}_{\text{gt}}^{(t,j)}|}, \quad (7)$$

where $\mathcal{M}_{\text{pred}}^{(t,j)}$ and $\mathcal{M}_{\text{gt}}^{(t,j)}$ are the binary masks of object j at frame t in the predicted and ground-truth videos, respectively. Higher SCS values indicate stronger structural alignment between the predicted and ground-truth sequences.

Figure 3 illustrates that SCS correlates strongly with correct action following, in contrast to perceptual metrics that emphasize visual realism. By focusing on structural evolution rather than appearance, SCS provides a principled,

Method	Frame 2			Frame 4			Frame 8			Frame 16		
	LPIPS↓	DreamSim↓	SCS↑	LPIPS↓	DreamSim↓	SCS↑	LPIPS↓	DreamSim↓	SCS↑	LPIPS↓	DreamSim↓	SCS↑
NWM	0.26	0.10	58.4	0.30	0.11	56.2	0.35	0.13	46.8	0.45	0.19	33.4
EgoWM (SVD)	0.25	0.10	62.0	0.27	0.10	61.7	0.31	0.12	57.2	0.39	0.17	55.2
EgoWM (Cosmos)	0.20	0.07	63.1	0.22	0.08	60.4	0.26	0.09	56.4	0.33	0.10	47.5

Table 1. Comparison with state-of-the-art methods on the RECON validation set after training on three navigation datasets. Each column group reports LPIPS, DreamSim, and SCS scores for different prediction horizons. Both of our variants outperform Navigation World Models, especially at longer horizons, highlighting the effectiveness of adapting pre-trained video diffusion models for world modeling.

quantitative measure of how faithfully a model predicts the causal consequences of an agent’s actions.

5. Experiments

Datasets and evaluation. We evaluate our approach across three progressively challenging settings — (i) classical ego-centric navigation in real-world robot environments, (ii) humanoid navigation, and (iii) humanoid manipulation with a 25-DoF action space — using four open-source datasets. RECON [38] contains diverse real-world indoor navigation trajectories. SCAND [20] features long, continuous paths through structured indoor environments, emphasizing smooth motion and spatial consistency. TartanDrive [39] includes challenging outdoor trajectories with uneven terrain and dynamic backgrounds, testing robustness to visual and proprioceptive noise. Finally, the 1X Humanoid Dataset [1] includes both navigation and manipulation episodes paired with 25-DoF joint-angle states, enabling evaluation of high-dimensional embodied control. All datasets are used for training, and we report quantitative results on the validation splits of RECON and 1X Humanoid.

Following prior work [7], we report the standard perceptual similarity metrics LPIPS [51] and DreamSim [13] to assess visual fidelity between predicted and ground-truth frames. To better capture differences in action following accuracy between the models, we additionally report our SCS metric introduced in Section 4.

Implementation details Across all experiments, we evaluate two variants of our method built on top of the SVD [8] and Cosmos [2] (Predict2-2B) models, and benchmark against Navigation World Models (NWM) [7], the only open-source ego-centric navigation baseline. For the SVD-based variant, we embed each action scalar using sine–cosine features followed by a small MLP for both 3-DoF navigation and 25-DoF humanoid control. For the Cosmos variant, we replace the sinusoidal features with a more expressive MLP to mitigate information loss caused by temporal compression. We use two 1D convolutional layers to downsample the action embeddings to match the temporally compressed latent resolution of Cosmos.

Fine-tuning is performed using the original pretraining objective of the base diffusion model (denoising or flow

matching; see Section 3.1), extended to include the additional action-conditioning pathway. The learning rate for the newly introduced action projection module is set to $10\times$ higher than that of the base model weights. Additional implementation and optimization details are provided in the appendix.

5.1. Navigation results

We fine-tune both variants of our method on the training sets of RECON, SCAND, and Tartan-Drive for a fair comparison with NWM and report results on the validation set of RECON. The SVD model is trained at 512×512 resolution to predict 8 future frames and evaluated autoregressively over two 8-frame chunks (16 frames total), while the Cosmos variant operates at 480×640 resolution and directly predicts 16 frames in a single forward pass.

Table 1 reports LPIPS, DreamSim, and our proposed SCS metrics for prediction horizons of 2 to 16 frames. Both variants of our method outperform NWM across all horizons and metrics, with especially large gains under the SCS metric and larger distance from the initial frame, confirming superior action alignment. Cosmos achieves higher perceptual fidelity, reflecting the stronger visual priors of its large-scale pretraining, whereas SVD demonstrates more stable structural consistency over longer trajectories due to the lack of temporal downsampling in its U-Net backbone.

Figure 4 visualizes predicted rollouts across all three navigation datasets. Both variants of our model produce realistic sequences that closely follow the provided trajectories, while NWM exhibits noticeable drift. Cosmos generates sharper and more detailed predictions, whereas SVD exhibits mild drift due to its autoregressive inference. Overall, our results demonstrate that leveraging pre-trained video diffusion models for world modeling yields substantial improvements over specialized NWM architecture, combining high perceptual quality with robust action following.

Since NWM is frame-wise autoregressive, it takes significantly longer to roll out sequences compared to our diffusion-based models, where we generate frames in a chunk together. The latency behavior is shown in Figure 5, where we can see that as the number of frames increases, NWM becomes as much as 6x slower compared to Cos-

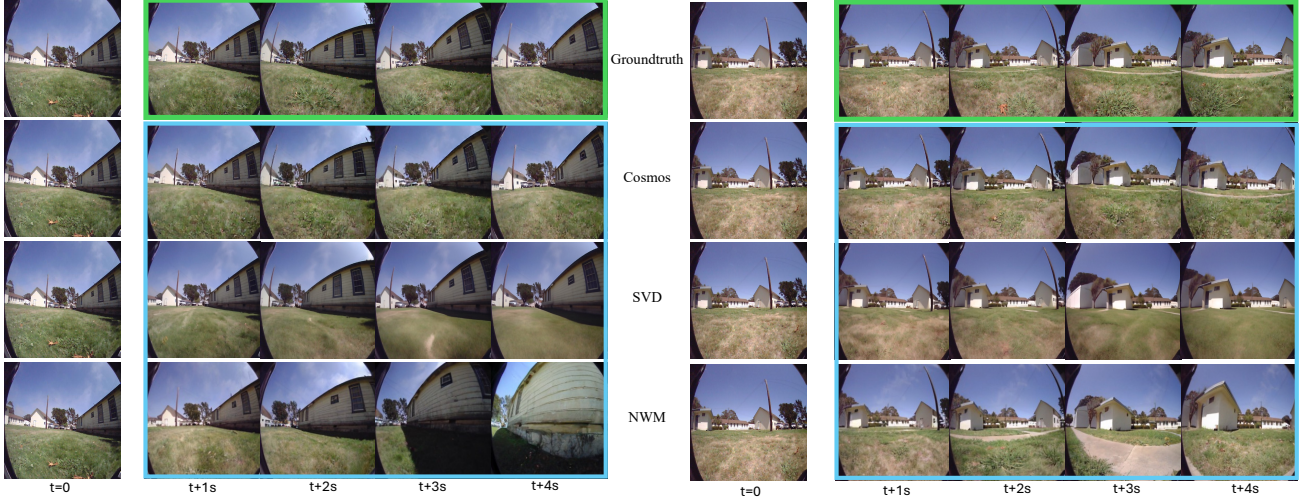


Figure 4. Qualitative results on ego-centric navigation. Both variants of our model generate realistic, temporally coherent sequences that accurately follow the provided action trajectories, while NWM exhibits noticeable drift (e.g., veering right in the first column).

Task	Variant	Frame 2			Frame 4			Frame 8			Frame 16		
		LPIPS↓	DreamSim↓	SCS↑	LPIPS↓	DreamSim↓	SCS↑	LPIPS↓	DreamSim↓	SCS↑	LPIPS↓	DreamSim↓	SCS↑
Navigation	SVD	0.11	0.07	75.6	0.16	0.09	66.4	0.26	0.13	50.3	0.35	0.18	34.4
	SVD (scratch)	0.17	0.15	69.7	0.25	0.20	56.0	0.37	0.30	40.0	0.47	0.40	21.6
	Cosmos	0.11	0.04	65.2	0.19	0.06	54.0	0.27	0.09	42.3	0.40	0.19	27.0
Manipulation	SVD	0.04	0.04	86.8	0.06	0.05	81.8	0.10	0.07	75.0	0.13	0.10	76.6
	Cosmos	0.04	0.03	86.2	0.07	0.05	82.0	0.10	0.06	78.2	0.12	0.07	67.7

Table 2. Results of SVD, Cosmos, and a variant of SVD trained from scratch on humanoid navigation and manipulation. The pre-trained SVD variant outperforms the baseline trained from scratch by significant margins, demonstrating the value of Internet-scale pre-training in this challenging scenario.

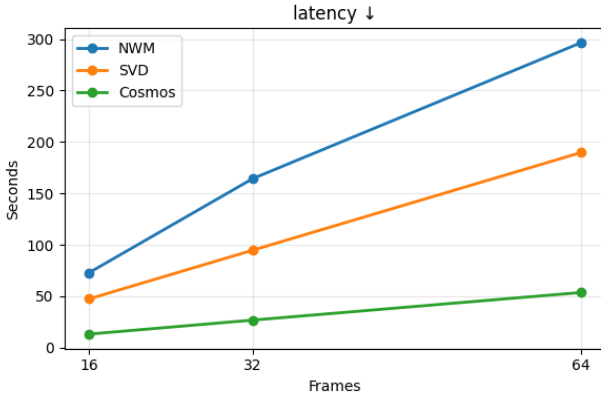


Figure 5. The inference latency of autoregressive NWM is much higher compared to SVD and Cosmos, and the gap becomes more pronounced as the number of frames increases.

mos. Cosmos is still faster than SVD since it can generate 64 frames at once, owing to its pre-training, whereas SVD can only generate 8-frame chunks auto-regressively.

5.2. Humanoid results

We next evaluate our approach on the 1X Humanoid Dataset, a significantly more challenging setting involv-

ing a 25-DoF control space spanning all major joints, neck motion, and gripper actions. The SVD model predicts 8 frames per step and infers 16 frames autoregressively, while Cosmos predicts 16 frames in a single pass. As shown in the 25-DoF navigation results in Table 2, both variants achieve comparable perceptual quality but exhibit slightly lower SCS scores toward the end of the trajectory compared to the 3-DoF navigation experiments. This reflects the increased difficulty of high-dimensional humanoid control, where maintaining coherent motion requires reasoning over many coupled joints and partial ego-centric visibility. Nevertheless, our universal conditioning approach applies to both embodiments without any architectural modifications, demonstrating its scalability across action spaces that differ by nearly an order of magnitude in complexity. The SVD model also outperforms its variant trained from scratch, with the gap being especially significant on perceptual similarity metrics, confirming the value of Internet-scale, passive pretraining. While the Cosmos variant outperforms the SVD variant trained from scratch on perceptual metrics, action following is slightly worse initially. However, as we go further into the future, Cosmos dominates.

In the lower part of Table 2, we also quantitatively evalu-

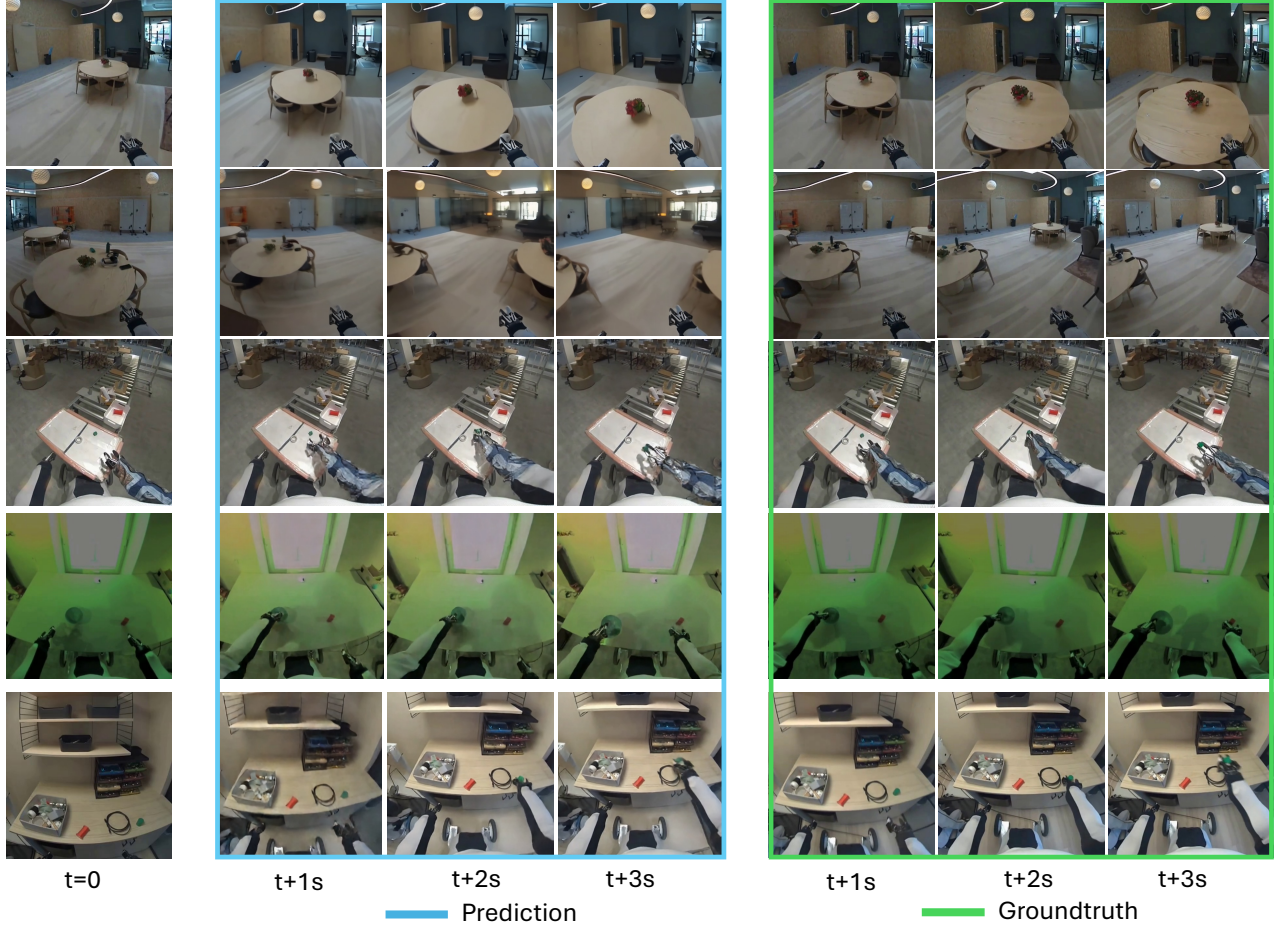


Figure 6. Our action-conditioned video world model enables a humanoid agent to navigate and execute long-horizon, contact-rich manipulation skills by conditioning on desired actions. Across diverse scenes and object geometries, the model produces physically consistent body motions, stable grasps, and smooth end-effector trajectories that closely follow the provided action sequence. The navigation results here are from SVD, and the manipulation results are from Cosmos. Results best viewed in our website egowm.github.io

ate the Cosmos and SVD variants at 25-DoF manipulation. Since the scene changes very little during manipulation as opposed to during navigation, the LPIPS and DreamSim scores are much lower even at frame 16, compared to navigation. We also see high SCS scores, showing that both variants learn to accurately follow the manipulation commands. SVD is better at action following than Cosmos, a common trend across all results, as a consequence of the temporal compression in Cosmos.

Figure 6 illustrates humanoid sequences. Despite the dramatic increase in embodiment complexity to 25 DoF, our model produces stable trajectories that remain consistent with the provided actions for navigation, reaching, and grasping. Our model maintains coherent global scene structure while capturing detailed arm, hand, and finger articulation throughout. Despite the high dimensionality of the control space, the predicted videos remain visually consistent and physically plausible — demonstrating that our approach extends naturally from navigation to fine-grained

manipulation without architectural modifications.

5.3. Generalization results

To test the limits of open-world generalization, we evaluate our model in visually non-realistic domains such as paintings. Specifically, we evaluate the SVD variant trained with the 3-DoF action space in the first three rows of Figure 7. Remarkably, this model demonstrates accurate action following despite the absence of any physical grounding or real-world dynamics. As shown in the figure, the model correctly interprets motion commands — navigating forward, turning, or rotating — while preserving the aesthetic and textural characteristics of the painted environment. This ability emerges purely from effectively harnessing Internet-scale pretraining, which endows the base diffusion models with broad world priors. In Figure 8, we also show that our 25-DoF humanoid navigation model can generalize to completely unseen real-world scenes captured in our lab, demonstrating the practical utility of our world model, even

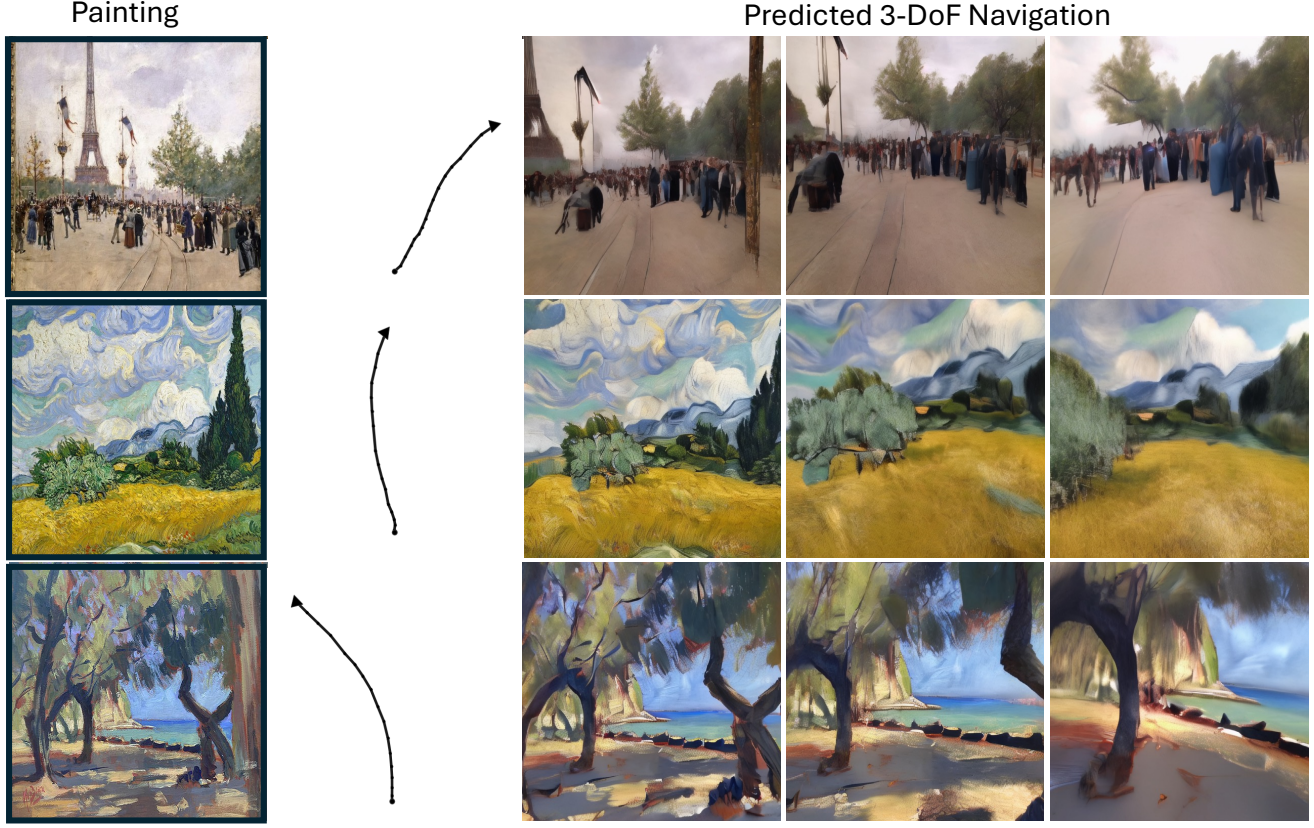


Figure 7. Our model generalizes to unrealistic visual domains, such as navigating inside paintings, while still accurately following action commands. Despite the drastic shift in appearance and lack of physical realism, the model preserves coherent motion and control, effectively “walking into” and through painted worlds by leveraging strong Internet-scale visual priors. These results are obtained with a 3-DoF SVD variant of our model. Results best viewed in our website egowm.github.io

under highly complex action spaces.

6. Conclusion

We presented a simple and general framework for transforming pre-trained video diffusion models into action-conditioned world models. By introducing lightweight action conditioning into existing architectures, our method leverages the broad priors learned from Internet-scale data to produce physically and semantically consistent futures. Through extensive experiments, we demonstrated strong generalization across diverse embodiments and environments, including humanoids with high-dimensional action spaces. Finally, we proposed the Structural Consistency Score (SCS) to faithfully evaluate world models’ action following. These contributions open a path toward scalable, controllable, and generalizable world models, bridging the gap between passive and active visual prediction.

Acknowledgment

This project was supported by Toyota Research Institute.

References

- [1] 1X Technologies. 1X World Model Challenge, 2024. [4](#), [6](#)
- [2] Niket Agarwal, Arslan Ali, Maciej Bala, Yogesh Balaji, Erik Barker, Tiffany Cai, Prithvijit Chattopadhyay, Yongxin Chen, Yin Cui, Yifan Ding, et al. Cosmos world foundation model platform for physical AI. *arXiv preprint arXiv:2501.03575*, 2025. [2](#), [3](#), [6](#), [13](#)
- [3] Eloi Alonso, Adam Jelley, Vincent Micheli, Anssi Kanervisto, Amos J Storkey, Tim Pearce, and François Fleuret. Diffusion for world modeling: Visual details matter in Atari. *NeurIPS*, 2024. [2](#), [3](#)
- [4] Mohammad Babaeizadeh, Chelsea Finn, Dumitru Erhan, Roy H Campbell, and Sergey Levine. Stochastic variational video prediction. *arXiv preprint arXiv:1710.11252*, 2017. [3](#)
- [5] Anurag Bagchi, Zhipeng Bao, Yu-Xiong Wang, Pavel Tolkmakov, and Martial Hebert. ReferEverything: Towards segmenting everything we can speak of in videos. In *ICCV*, 2025. [3](#)
- [6] Jianhong Bai, Menghan Xia, Xiao Fu, Xiantao Wang, Lianrui Mu, Jinwen Cao, Zuozhu Liu, Haoji Hu, Xiang Bai, Pengfei Wan, et al. ReCamMaster: Camera-controlled generative rendering from a single video. In *ICCV*, 2025. [3](#)



Figure 8. Our method generalizes to real-world scenes captured in our campus, while following 25-DoF navigation commands. Here we show two ground-truth navigation trajectories (in the first and third rows) acted out in the same real-world scene (in the second and fourth rows, respectively). In the first trajectory, the humanoid moves slightly forward and then turns right; and in the second trajectory, the humanoid turns right and then moves forward. These results are obtained with a 25-DoF SVD variant of our model.

- [7] Amir Bar, Gaoyue Zhou, Danny Tran, Trevor Darrell, and Yann LeCun. Navigation world models. In *CVPR*, 2025. 2, 3, 5, 6, 13
- [8] Andreas Blattmann, Tim Dockhorn, Sumith Kulal, Daniel Mendelevitch, Maciej Kilian, Dominik Lorenz, Yam Levi, Zion English, Vikram Voleti, Adam Letts, et al. Stable video diffusion: Scaling latent video diffusion models to large datasets. *arXiv preprint arXiv:2311.15127*, 2023. 3, 6, 13
- [9] João Carreira and Andrew Zisserman. Quo vadis, action recognition? a new model and the kinetics dataset. In *CVPR*, 2017. 3
- [10] Haoxin Chen, Yong Zhang, Xiaodong Cun, Menghan Xia, Xintao Wang, Chao Weng, and Ying Shan. VideoCrafter2: Overcoming data limitations for high-quality video diffusion models. In *CVPR*, 2024. 3
- [11] Frederik Ebert, Chelsea Finn, Sudeep Dasari, Annie Xie, Alex Lee, and Sergey Levine. Visual foresight: Model-based deep reinforcement learning for vision-based robotic control.

arXiv preprint arXiv:1812.00568, 2018. 3

[12] Mark Everingham, Luc Van Gool, Christopher KI Williams, John Winn, and Andrew Zisserman. The PASCAL visual object classes (VOC) challenge. *International Journal of Computer Vision*, 88(2):303–338, 2010. 5

[13] Stephanie Fu, Netanel Tamir, Shobhita Sundaram, Lucy Chai, Richard Zhang, Tali Dekel, and Phillip Isola. Dream-Sim: Learning new dimensions of human visual similarity using synthetic data. In *NeurIPS*, 2023. 5, 6

[14] Yanjiang Guo, Lucy Xiaoyang Shi, Jianyu Chen, and Chelsea Finn. Ctrl-world: A controllable generative world model for robot manipulation, 2025. 2, 3, 4

[15] David Ha and Jürgen Schmidhuber. World models. In *NeurIPS*, 2018. 2, 3

[16] Adam W. Harley, Yang You, Xinglong Sun, Yang Zheng, Nikhil Raghuraman, Yunqi Gu, Sheldon Liang, Wen-Hsuan Chu, Achal Dave, Pavel Tokmakov, Suya You, Rares Ambrus, Katerina Fragkiadaki, and Leonidas J. Guibas. All-Tracker: Efficient dense point tracking at high resolution. In *ICCV*, 2025. 5

[17] Haoyang He, Jay Patrikar, Dong-Ki Kim, Max Smith, Daniel McGann, Ali akbar Agha-mohammadi, Shayegan Omidshafiei, and Sebastian Scherer. Grndctr: Grounding world models via self-supervised reward alignment, 2025. 2, 3

[18] Jonathan Ho, William Chan, Chitwan Saharia, Jay Whang, Ruiqi Gao, Alexey Gritsenko, Diederik P Kingma, Ben Poole, Mohammad Norouzi, David J Fleet, et al. ImaGen Video: High definition video generation with diffusion models. *arXiv preprint arXiv:2210.02303*, 2022. 3

[19] Yucheng Hu, Yanjiang Guo, Pengchao Wang, Xiaoyu Chen, Yen-Jen Wang, Jianke Zhang, Koushil Sreenath, Chaochao Lu, and Jianyu Chen. Video prediction policy: A generalist robot policy with predictive visual representations. In *ICML*, 2025. 3

[20] Haresh Karnan, Anirudh Nair, Xuesu Xiao, Garrett Warrell, Sören Pirk, Alexander Toshev, Justin Hart, Joydeep Biswas, and Peter Stone. Socially compliant navigation dataset (scand): A large-scale dataset of demonstrations for social navigation. *IEEE Robotics and Automation Letters*, 7(4):11807–11814, 2022. 6, 13

[21] Bingxin Ke, Anton Obukhov, Shengyu Huang, Nando Metzger, Rodrigo Caye Daudt, and Konrad Schindler. Repurposing diffusion-based image generators for monocular depth estimation. In *CVPR*, 2024. 3

[22] Seung Wook Kim, Yuhao Zhou, Jonah Philion, Antonio Torralba, and Sanja Fidler. Learning to simulate dynamic environments with GameGAN. In *CVPR*, 2020. 3

[23] Diederik P Kingma and Max Welling. Auto-encoding variational bayes. *arXiv preprint arXiv:1312.6114*, 2013. 4

[24] Junbang Liang, Pavel Tokmakov, Ruoshi Liu, Sruthi Sudhakar, Paarth Shah, Rares Ambrus, and Carl Vondrick. Video generators are robot policies. *arXiv preprint arXiv:2508.00795*, 2025. 3

[25] Ruoshi Liu, Rundi Wu, Basile Van Hoorick, Pavel Tokmakov, Sergey Zakharov, and Carl Vondrick. Zero-1-to-3: Zero-shot one image to 3D object. In *ICCV*, 2023. 3

[26] Yaofang Liu, Xiaodong Cun, Xuebo Liu, Xintao Wang, Yong Zhang, Haoxin Chen, Yang Liu, Tieyong Zeng, Raymond Chan, and Ying Shan. EvalCrafter: Benchmarking and evaluating large video generation models. In *CVPR*, 2024. 2

[27] James L. Mannos and David J. Sakrison. The effects of a visual fidelity criterion on the encoding of images. *IEEE Trans. Information Theory*, 20(4):525–536, 1974. 3

[28] Daniel McNamee and Daniel M Wolpert. Internal models in biological control. *Annual review of control, robotics, and autonomous systems*, 2(1):339–364, 2019. 2

[29] Junhyuk Oh, Xiaoxiao Guo, Honglak Lee, Richard L Lewis, and Satinder Singh. Action-conditional video prediction using deep networks in Atari games. *NeurIPS*, 2015. 3

[30] Ege Ozguroglu, Ruoshi Liu, Dídac Suris, Dian Chen, Achal Dave, Pavel Tokmakov, and Carl Vondrick. pix2gestalt: Amodal segmentation by synthesizing wholes. In *CVPR*, 2024. 3

[31] Jing-Cheng Pang, Nan Tang, Kaiyuan Li, Yuting Tang, Xin-Qiang Cai, Zhen-Yu Zhang, Gang Niu, Masashi Sugiyama, and Yang Yu. Learning view-invariant world models for visual robotic manipulation. In *ICLR*, 2025. 3

[32] William Peebles and Saining Xie. Scalable diffusion models with transformers. In *ICCV*, 2023. 2, 3, 4

[33] Giovanni Pezzulo, Thomas Parr, and Karl Friston. Active inference as a theory of sentient behavior. *Biological Psychology*, 186:108741, 2024. 2

[34] Nikhila Ravi, Valentin Gabeur, Yuan-Ting Hu, Ronghang Hu, Chaitanya Ryali, Tengyu Ma, Haitham Khedr, Roman Rädle, Chloe Rolland, Laura Gustafson, et al. SAM 2: Segment anything in images and videos. In *ICLR*, 2025. 5

[35] Robin Rombach, Andreas Blattmann, Dominik Lorenz, Patrick Esser, and Björn Ommer. High-resolution image synthesis with latent diffusion models. In *CVPR*, 2022. 4

[36] Olaf Ronneberger, Philipp Fischer, and Thomas Brox. U-Net: Convolutional networks for biomedical image segmentation. In *MICCAI*, 2015. 2, 3, 4

[37] Younggyo Seo, Danijar Hafner, Hao Liu, Fangchen Liu, Stephen James, Kimin Lee, and Pieter Abbeel. Masked world models for visual control. In *CoRL*, 2023. 2

[38] Dhruv Shah, Benjamin Eysenbach, Gregory Kahn, Nicholas Rhinehart, and Sergey Levine. Rapid exploration for open-world navigation with latent goal models. In *CoRL*, 2021. 6

[39] Samuel Triest, Matthew Sivaprakasam, Sean J Wang, Wenshan Wang, Aaron M Johnson, and Sebastian Scherer. Tar-tanDrive: A large-scale dataset for learning off-road dynamics models. In *ICRA*, 2022. 6, 13

[40] Alexander Unterthiner, Sjoerd van Steenkiste, Daniel Keyser, Thomas Kipf, Alexander D’Amour, Peter Sorrenson, and Olivier Bousquet. Towards accurate generative models of video: A new metric and challenges. In *NeurIPS*, 2018. 2, 3

[41] Dani Vavlevski, Yaniv Leviathan, Moab Arar, and Shlomi Fruchter. Diffusion models are real-time game engines. *arXiv preprint arXiv:2408.14837*, 2024. 2, 3

[42] Basile Van Hoorick, Rundi Wu, Ege Ozguroglu, Kyle Sargent, Ruoshi Liu, Pavel Tokmakov, Achal Dave, Changxi

Zheng, and Carl Vondrick. Generative camera dolly: Extreme monocular dynamic novel view synthesis. In *ECCV*, 2024. 3

[43] Team Wan, Ang Wang, Baole Ai, Bin Wen, Chaojie Mao, Chen-Wei Xie, Di Chen, Feiwu Yu, Haiming Zhao, Jianxiao Yang, et al. Wan: Open and advanced large-scale video generative models. *arXiv preprint arXiv:2503.20314*, 2025. 3

[44] Juniu Wang, Hangjie Yuan, Dayou Chen, Yingya Zhang, Xiang Wang, and Shiwei Zhang. ModelScope text-to-video technical report. *arXiv preprint arXiv:2308.06571*, 2023. 3

[45] Xiaofeng Wang, Zheng Zhu, Guan Huang, Xinze Chen, Jia-gang Zhu, and Jiwen Lu. Drivedreamer: Towards real-world-drive world models for autonomous driving. In *ECCV*, 2024. 2

[46] Yunbo Wang, Haixu Wu, Jianjin Zhang, Zhifeng Gao, Jian-min Wang, Philip S Yu, and Mingsheng Long. PredRNN: A recurrent neural network for spatiotemporal predictive learning. *IEEE Transactions on Pattern Analysis and Machine Intelligence*, 45(2):2208–2225, 2022. 3

[47] Zhou Wang, Alan C. Bovik, Hamid R. Sheikh, and Eero P. Simoncelli. Image quality assessment: from error visibility to structural similarity. *IEEE Trans. Image Processing*, 13(4):600–612, 2004. 3

[48] Charith Wickrema, Sara Leary, Shivangi Sarkar, Mark Giglio, Eric Bianchi, Eliza Mace, and Michael Twardowski. Benchmarking image similarity metrics for novel view synthesis applications. *arXiv preprint arXiv:2506.12563*, 2025. 2

[49] Thaddäus Wiedemer, Yuxuan Li, Paul Vicol, Shixiang Shane Gu, Nick Matarese, Kevin Swersky, Been Kim, Priyank Jaini, and Robert Geirhos. Video models are zero-shot learners and reasoners. *arXiv preprint arXiv:2509.20328*, 2025. 2

[50] Zhuoyi Yang, Jiayan Teng, Wendi Zheng, Ming Ding, Shiyu Huang, Jiazheng Xu, Yuanming Yang, Wenyi Hong, Xiaohan Zhang, Guanyu Feng, et al. Cogvideox: Text-to-video diffusion models with an expert transformer. In *ICLR*, 2025. 3

[51] Richard Zhang, Phillip Isola, Alexei A Efros, Eli Shechtman, and Oliver Wang. The unreasonable effectiveness of deep features as a perceptual metric. In *CVPR*, 2018. 2, 3, 5, 6

[52] Wenliang Zhao, Yongming Rao, Zuyan Liu, Benlin Liu, Jie Zhou, and Jiwen Lu. Unleashing text-to-image diffusion models for visual perception. In *ICCV*, 2023. 3

[53] Chuning Zhu, Raymond Yu, Siyuan Feng, Benjamin Burchfiel, Paarth Shah, and Abhishek Gupta. Unified world models: Coupling video and action diffusion for pretraining on large robotic datasets. In *RSS*, 2025. 2, 3

[54] Fangqi Zhu, Hongtao Wu, Song Guo, Yuxiao Liu, Chilam Cheang, and Tao Kong. IRASim: A fine-grained world model for robot manipulation. In *ICCV*, 2025. 2, 3, 4

[55] Zixin Zhu, Xuelu Feng, Dongdong Chen, Junsong Yuan, Chunming Qiao, and Gang Hua. Exploring pre-trained text-to-video diffusion models for referring video object segmentation. In *ECCV*, 2024. 3

Appendix

In this appendix, we report additional results, details, and visualizations. We begin by discussing our Structural Consistency Metric in Section A. Next, we report further implementation details of our approach in Section B and provide data, compute, latency, and resolution comparisons with the Navigation World Models (NWM) [7]. Finally, we discuss some failure modes of our method in Section C.

A. Structural Consistency Evaluation

In Figure 9 we qualitatively demonstrate the structural consistency evaluation using our SCS metric, for navigation and manipulation. The first row shows predicted frames for 3-DoF navigation in RECON, with two key structures (a house and a tree) tracked with blue masks, and the positions of these structures in the corresponding ground-truth frames shown with red masks. As we can see, initially the two structures’ predicted location and shape is perfectly aligned with ground-truth but as we go further into the future, the imperfections in the action following behavior results in a drift. The second row shows similar evaluation for 25-DoF manipulation using humanoid. Note here that while the hand’s predicted motion is very close to the ground-truth, the shape of the cup gets distorted during manipulation, and will be correctly penalized by our SCS metric.

Finally in the bottom two rows, we show structural consistency evaluation in case of highly distorted predictions. The third row shows distorted 25-DoF navigation predictions from an intermediate stage of model training and the last row shows the distorted light fixture and table tracked using blue masks, with ground-truth positions in red as before. As we can see, SAM2 mask tracking is robust to distortions in the generated frames and therefore our SCS metric can evaluate action following even when the fidelity of the generation is poor, which highlights our intended disentanglement of action following from visual quality.

B. Implementation Details

Training details. We train both our SVD [8] and Cosmos [2] models on 8 A100 GPUs for all variants. For the SVD variant, we take a learning rate of 1e-5 for all the model parameters except the action projection layers, where we adopt a larger learning rate of 1e-4. For the Cosmos variant, we use a learning rate of 1e-6 for the other parameters and 1e-5 for the action projection layers. Our longest training run takes 8 days for our Cosmos-2B training for 25 DoF manipulation on the 1x dataset, which has 100 hours of training videos at 30 FPS. We subsample the frames at 5 FPS for both training and inference. For 1x training, we select continuous frame sequences with a stride

of 5. For training on 3-DoF datasets, we use a stride of 1 for SCAND [20] and Tartan [39], and a stride of 5 for RECON.

Comparison with NVM. Table 3 lists the action datasets and compute resources used for training each method. NWM employs a higher-resolution version of the Huron dataset, which we did not have access to. While NWM is trained on 64 H100 GPUs, both our SVD and Cosmos variants are trained on only 8 A100s. While NWM predicts frames at 224×224 , we predict at 512×512 for SVD and 480×640 for Cosmos. For fairness, we compute all metrics at 224×224 by downsampling our predictions. Despite using less action data and approximately $8\times$ less compute, our models outperform NWM.

To generate the latency plot shown in Figure 5 of the main paper, we perform inference on the same 20 RECON samples across varying prediction horizons, using each model’s native resolution – 224×244 for NWM, 512×512 for Ours (SVD), and 480×640 for Ours (Cosmos). All inferences are executed on a single A100 GPU. Our models achieve up to $6\times$ faster inference speed while predicting at up to $2\times$ higher resolution.

C. Failure Modes

C.1. Manipulation

Our model struggles to generate small manipulated objects in a physically consistent manner, particularly when object shapes must be preserved across occlusions. Maintaining object permanence during complex manipulation also remains challenging. In the first two rows of Fig 10, we illustrate one such failure case, where the square shaped block gets distorted during manipulation. We attribute these issues primarily to limitations of the underlying video generation backbones and expect that future advances in video generative modeling will improve these aspects of world-modeling performance.

C.2. Generalization

While our generalisation results in extremely OOD painting scenes are quite impressive for our SVD backbone, we find that the Cosmos variant is more prone to collapse, where the generation results change the painting scene to a completely different real-world scene, as shown in the last row of Fig 10. We think that the reason this issue is far more frequent in the Cosmos model is largely due to the pre-training data distribution, which is more focused on real-world, physical data in case of Cosmos. We also see some failure modes in the SVD variant, where the generated scene loses fidelity in some cases, where the model has to imagine large parts of the scene quickly as a result of the navigation commands, or in generating people or structures consistently through-out the video, where some structures might vanish, appear or morph into some other structures. One

Method	3-DoF Action Data	Compute	Resolution	Avg. 64f Latency (s)
NWM	RECON, SCAND, Tartan-Drive, Huron	64x H100s	224x224	≈ 300
Ours (SVD)	RECON, SCAND, Tartan-Drive	8x A100s	512x512	≈ 200
Ours (Cosmos)			480x640	≈ 50

Table 3. Comparison of data, compute, resolution, and latency with NWM for 3-DoF position control.

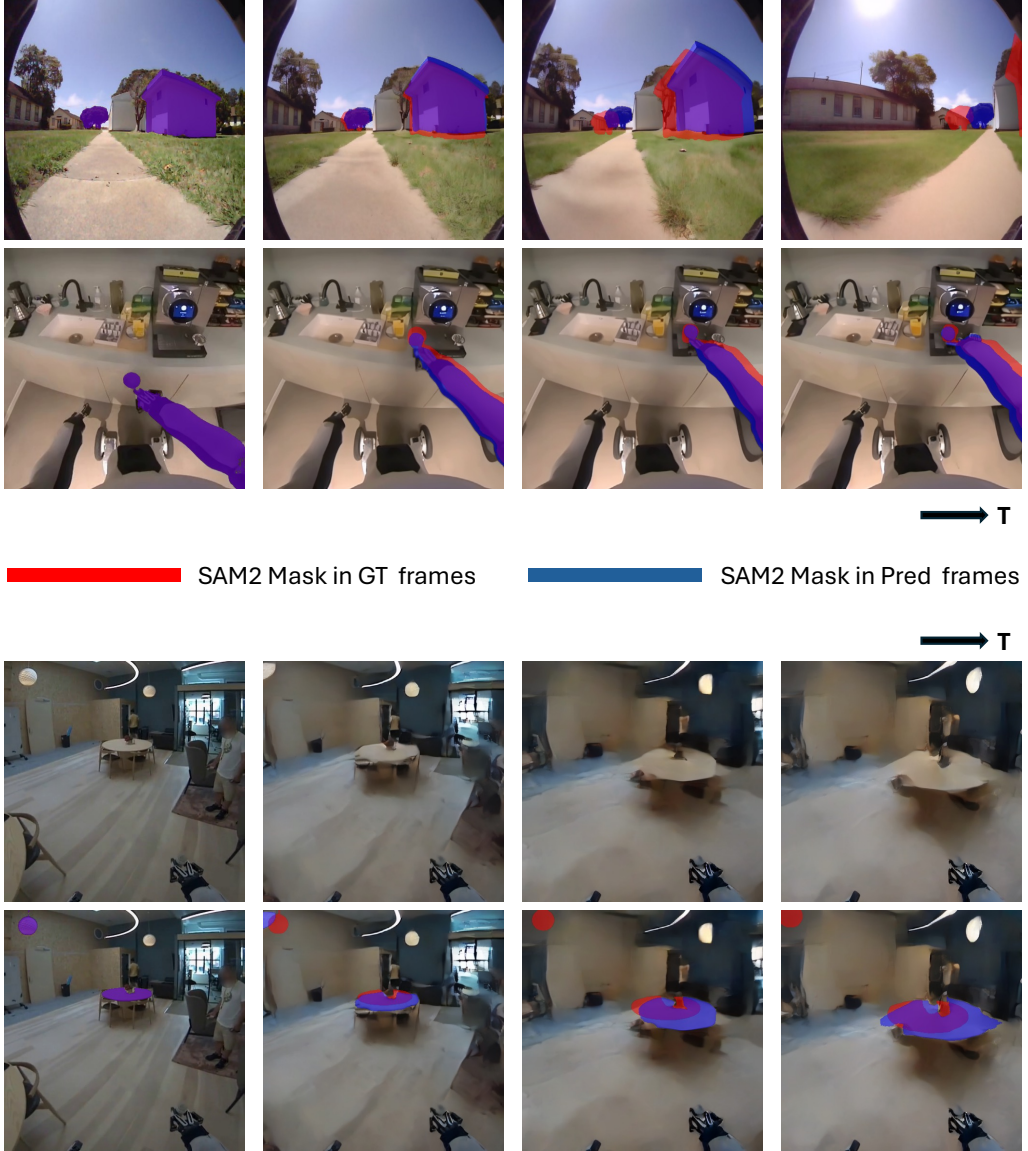


Figure 9. This is an illustration of our SCS metric computation. The first two rows show the difference between predicted locations of structures and their groundtruth location for navigation and manipulation. The last two rows demonstrate the robustness of our metric to distorted generations, with the third row showing the distorted predicted frames and the final row showing the tracked masks of these distorted structures and their groundtruth positions.

such instance of structural inconsistency is demonstrated in the third row of Fig 10. We believe the failure modes seen in SVD, can be solved as the base models get better and be-

come capable of consistent longer term generation. However, improving structural consistency using post-training techniques remains an interesting direction for the future.

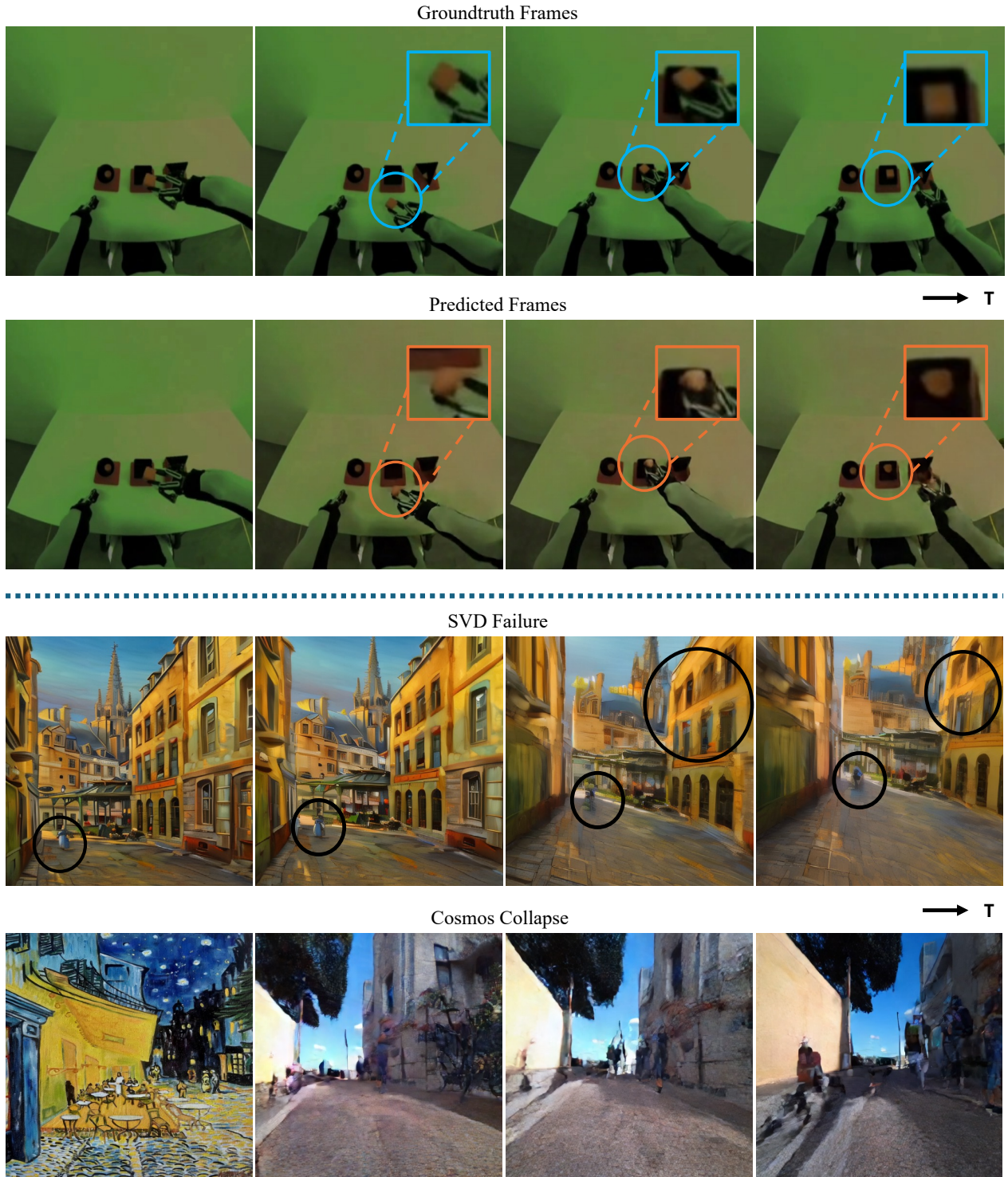


Figure 10. Failure modes of our world model. In the first two rows we show shape inconsistencies in our manipulation results, in the third row we show structural inconsistencies in our SVD 3-DoF navigation world model’s painting generalizations and in the last row we show collapse to a real-world scene in our Cosmos 3-DoF navigation world model.